

# Phase measurements of EUV mask defects

Rene A. Claus<sup>a</sup>, Yow-Gwo Wang<sup>b</sup>, Antoine Wojdyla<sup>c</sup>, Markus P. Benk<sup>c</sup>, Kenneth A. Goldberg<sup>c</sup>, Andrew R. Neureuther<sup>b</sup>, Patrick P. Naulleau<sup>c</sup>, and Laura Waller<sup>b</sup>

<sup>a</sup>Applied Science and Technology, University of California, Berkeley;

<sup>b</sup>EECS, University of California, Berkeley;

<sup>c</sup>Center for X-ray Optics, Lawrence Berkeley National Laboratory

## ABSTRACT

Extreme Ultraviolet (EUV) Lithography mask defects were examined on the actinic mask imaging system, SHARP, at Lawrence Berkeley National Laboratory. A quantitative phase retrieval algorithm based on the Weak Object Transfer Function was applied to the measured through-focus aerial images to examine the amplitude and phase of the defects. The accuracy of the algorithm was demonstrated by comparing the results of measurements using a phase contrast zone plate and a standard zone plate. Using partially coherent illumination to measure frequencies that would otherwise fall outside the numerical aperture (NA), it was shown that some defects are smaller than the conventional resolution of the microscope. Programmed defects of various sizes were measured and shown to have both an amplitude and a phase component that the algorithm is able to recover.

**Keywords:** Extreme Ultraviolet Lithography, Multilayer Defect, Phase Defect, Quantitative Phase Imaging, Weak Object Transfer Function

## 1. INTRODUCTION

The availability of defect-free mask blanks for Extreme Ultraviolet (EUV) lithography is one of the big challenges facing EUV.<sup>1</sup> Particles that fall on the mask before or during multilayer deposition or pits that form during polishing of the substrate, are covered and behave as phase objects during printing. Several methods have been proposed to mitigate the effect of these defects during printing.<sup>2,3</sup> To properly evaluate and then compensate for a defect, it is necessary to know how it behaves. This can be done using modeling or by measuring the phase and amplitude of the defect.

We present measurements of the phase and amplitude of native and programmed EUV mask defects using a newly developed phase retrieval algorithm on aerial image measurements taken with the actinic EUV microscope, SHARP, at Lawrence Berkeley National Laboratory.<sup>4</sup> The algorithm is able to consider partially coherent illumination allowing it to more closely match the illumination used during wafer printing while also providing potentially higher throughput.<sup>5</sup> We show that the algorithm accurately recovers the defect by measuring the same native defect with two different zone plate lenses—a phase contrast lens and a standard zone plate. By varying the illumination, we show that it is likely that defects are significantly limited by the numerical aperture (NA) of the microscope. Finally we examined a series of programmed defects of different sizes to determine their phase and amplitude. We found that there was a relationship between the amplitude of defects and their phase. Larger defects had significant absorption—as high as 50%.

## 2. ALGORITHM

The algorithm we used is based on the Weak Object Assumption (WOA)<sup>6</sup> and can fully consider the interaction of the NA and illumination. The WOA assumes that the sample is weakly scattering so that the intensity variations depend primarily on the interference between the unscattered light (the DC of the object) and scattered light—the

Further author information: (Send correspondence to Rene A. Claus)  
Rene A. Claus: E-mail: reneclaus@gmail.com, Telephone: 1 949 334 7363

interference between scattered light and itself is assumed to be negligible. Under this assumption the measured intensity can be described by the linear sum of two convolutions as in Equation 1

$$I = I_0 + E_{re} * K_{re} + E_{im} * K_{im} + I_e \quad (1)$$

$$\widetilde{K}_{re} = \left( \widetilde{P} \cdot \widetilde{J} \right) \star \widetilde{P} + \widetilde{P} \star \left( \widetilde{P} \cdot \widetilde{J} \right) \quad (2)$$

$$\widetilde{K}_{im} = \left( \widetilde{P} \cdot \widetilde{J} \right) \star \widetilde{P} - \widetilde{P} \star \left( \widetilde{P} \cdot \widetilde{J} \right) \quad (3)$$

where  $I$  is the measured intensity,  $E_{re}$  is the real part of the object minus the DC,  $E_{im}$  is the imaginary part of the object,  $I_e$  is the error in the approximation, a variable with a *tilde* represent the Fourier transform of that variable,  $\widetilde{P}$  is the pupil function,  $\widetilde{J}$  is the source intensity distribution, and  $\widetilde{K}_{re}$  and  $\widetilde{K}_{im}$  are the Weak Object Transfer Functions (WOTF) for the real and imaginary parts of the object, respectively.

Using two or more measured intensities with different WOTFs, Equation 1 can be inverted to recover the object electric field. Since the transfer functions,  $K_{re}$  and  $K_{im}$ , include the source intensity distribution and the pupil function, the algorithm will work under arbitrary illumination and with any pupil function. The only requirement is that enough measurements are made that the equation can be inverted. A through-focus measurement series, as used in this paper, is sufficient to invert the equation because it produces different  $K_{re}$  and  $K_{im}$ . The WOA requires that  $|E_{re} + iE_{im}| \ll 1$ . This restriction is relaxed through an iterative approach by assuming the WOA holds, computing an estimate of  $E_{re}$  and  $E_{im}$ , computing  $I_e$ , the error in the WOA, using the current estimate of  $E_{re}$  and  $E_{im}$ , and subtracting that error from the inputs. Since the WOA assumes we can ignore  $I_e$ , this improves the recovery because after each iteration the remaining error is reduced. A more detailed explanation of the algorithm is being prepared for publication.<sup>5</sup>

### 3. EXPERIMENTAL VERIFICATION

To verify that the phase and amplitude recovered by the field are accurate and consistent with the defect on the mask as seen through the microscope, we measured the same native defect using two different lenses. SHARP uses zone plates as the objective lens, making it relatively easy to change the lens used for imaging. We used a 0.0825 NA lens with 13.5 nm light and a modified, phase contrast lens that had a 90° phase shifting region of radius 0.3 NA. Images of the same defect were taken under  $\sigma = 0.25$  monopole illumination through focus in the range  $\pm 5 \mu\text{m}$ . A subset of the images are shown in Figure 1. The phase contrast zone plate considerably changes how the defect and surrounding roughness appear in the aerial image. The speckle caused by the surrounding roughness, in particular, has significantly different contrast.

When the algorithm is applied to each through-focus series independently, it is expected to produce the same amplitude and phase since the underlying object on the mask is the same. The recovered fields are shown in Figure 2. The defect had a maximum effective height calculated by  $height = phase \cdot \lambda / 4\pi$  height of 2.5 nm and 70% absorption. The difference between the amplitude and phase recovered was smaller than 0.15 nm and 9%, respectively. Since the error is only 6% of the effective height and 12% of the amplitude, we conclude that the result corresponds to the true phase and amplitude of the object. This indicates the algorithm works even when using a complicated pupil function and partially coherent illumination.

### 4. IMPROVED RESOLUTION

In photolithography, off-axis sources are commonly used to get better resolution and print smaller features than an imaging system would otherwise allow. This means that some of the high frequency information that would ordinarily pass outside the NA is steered into the pupil. To properly model how a defect will print under these conditions, it should be measured using a higher NA or, alternatively, be measured using similar illumination. The algorithm is able to take advantage of the higher frequencies being captured using partially coherent illumination to recover the object with an effectively higher NA.

To check whether it is necessary to measure defects using higher resolution, we checked how they appear under different coherence. If the defect appears differently it indicates that a higher resolution measurement is needed. We measured a small defect with coherent,  $\sigma = 0.25$ , and  $\sigma = 0.45$  monopole illumination (shown in Figure

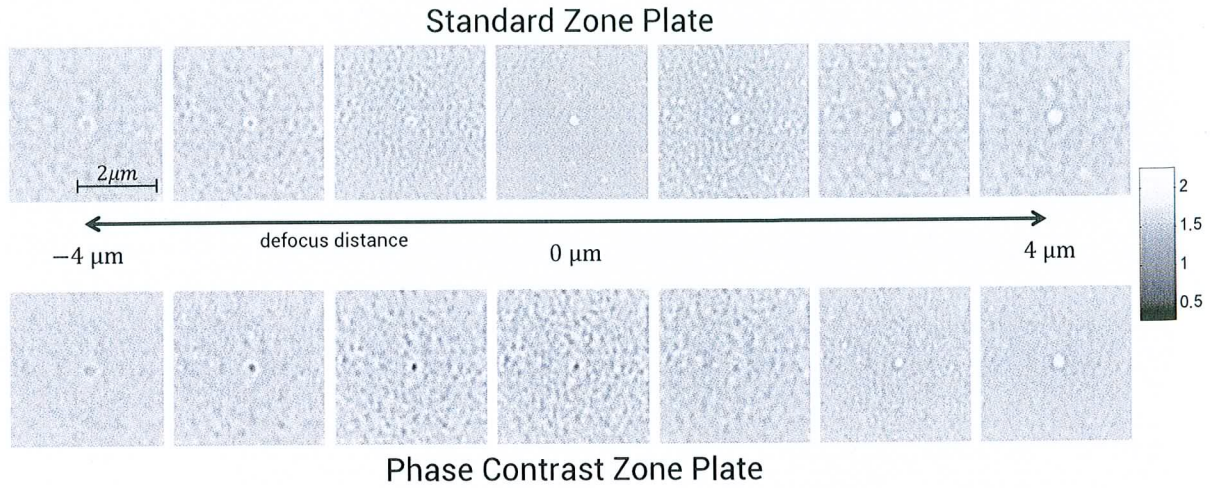


Figure 1. Aerial images of the same through-focus defect taken using a standard zone plate and a phase contrast zone plate produce very different images. Phase contrast causes the phase roughness to produce strong contrast at focus and changes the behavior of the defect through focus, which is described by the WOTF.

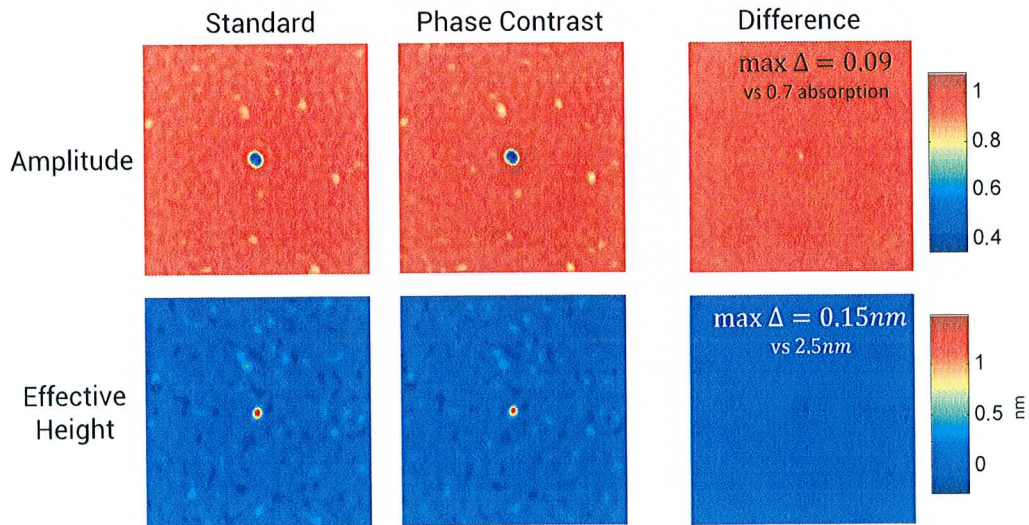


Figure 2. The amplitude and phase extracted from the standard zone plate measurements and the phase contrast zone plate measurements are nearly the same. The minimum amplitude was 0.3 while the maximum difference in the two amplitudes was only 0.09. The maximum phase (in effective height) was 2.5 nm and the maximum difference only 0.15 nm. This suggests that the algorithm recovered the true phase and amplitude of the defect, since the datasets going into the algorithm were qualitatively different yet produced nearly the same result.

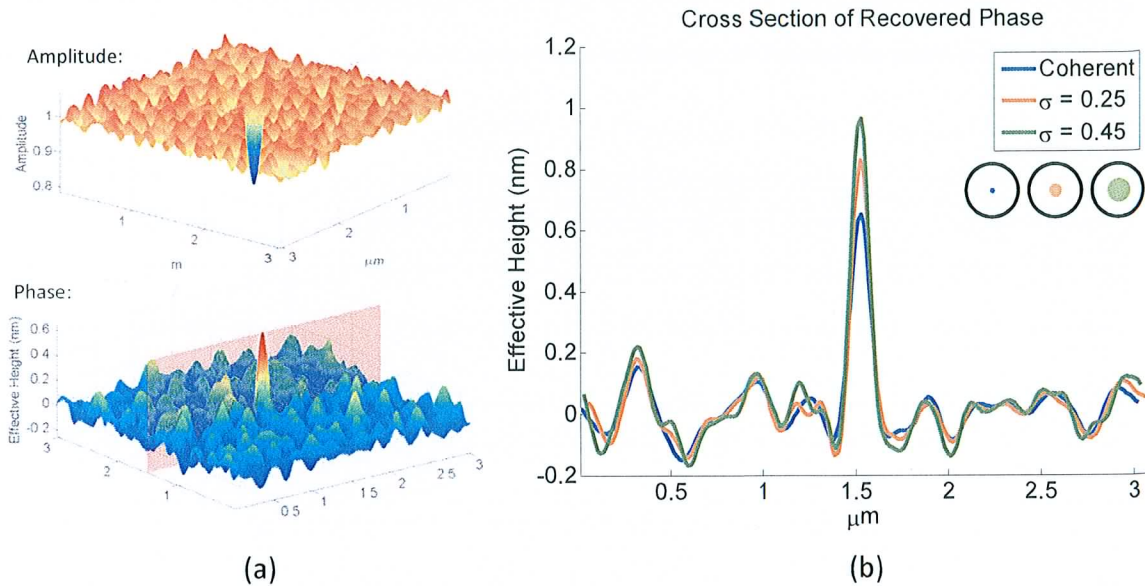


Figure 3. (a) recovered phase and amplitude of a small defect measured using coherent illumination, (b) comparison of the recovered phase along the red plane for coherent,  $\sigma = 0.25$  monopole illumination, and  $\sigma = 0.5$  monopole illumination. Larger source shapes allow spatial frequencies that would otherwise be filtered by the limited NA to be measured, resulting in higher effective resolution. This causes the height of the defect to approach the true size of the defect on the mask. The roughness is the same in each case because it is not limited by the NA.

3b). The NA used was 0.0825 and the wavelength was 13.5 nm. Figure 3b shows the cross section of the phase for each illumination. The cross section is shown on the 2D recovered phase in Figure 3a. We found that the peak recovered phase increases as the source shape grows. This is expected if the image of the defect is being significantly limited by the NA (the defect is smaller than the point spread function). More of the object frequencies are recovered when using the higher sigma measurements. Note that the surrounding roughness is consistent for all three measurements. This is expected if the roughness is not significantly limited by the NA. The consistency of the recovered roughness provides strong evidence that the algorithm is indeed recovering the true phase with improved resolution for larger source shapes.

## 5. AMPLITUDE AND PHASE DEFECTS

We examined the phase and amplitude of programmed defects of various sizes. These programmed defects have previously been studied using various techniques.<sup>7-9</sup> They consist of squares of fixed height and varied width patterned onto the substrate before multilayer deposition. We imaged the defects using  $\sigma = 0.25$  monopole illumination, an NA of 0.0825, and wavelength of 13.5 nm. The resulting peak amplitude and phase are plotted in Figure 4. AFM measurements of these programmed defects were only able to detect defects as small as 50 nm wide (on the substrate) due to surface roughness. Since the EUV light penetrates into the multilayer, defects as small as 40 nm (on the substrate) were visible in the aerial images. The measurements revealed that the large programmed defects have a significant amplitude component. This may be due to the bandlimiting of the NA or due to the multilayer growth process introducing reflectivity changes. Note that the native defects shown in Section 3 and Section 4 showed a similar amplitude component. The source of this amplitude is a subject of future study.

## 6. CONCLUSION

We have developed an algorithm based on the Weak Object Transfer Function that is able to recover the phase and amplitude of an object from a series of through-focus aerial images while considering the pupil function and

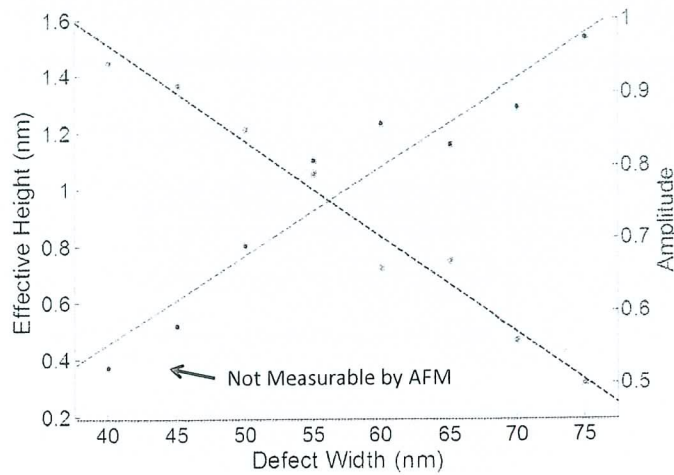


Figure 4. The maximum amplitude and phase (represented as  $height = phase \cdot \lambda/4\pi$ ) of programmed defects relative to the surrounding area is plotted vs. the width of the defect on the substrate. Larger defects showed considerable absorption in addition to phase. Defects smaller than the AFM resolution were visible under imaging.

partial coherence. We verified the algorithm using measurements of EUV multilayer defects taken on SHARP using a standard zone plate and a phase contrast zone plate. Nearly identical results from both measurements, despite very different inputs, indicates that the algorithm recovered the true phase and amplitude as seen from the camera.

Measurements taken using different illuminations show that measurements of blank defects are limited by the NA. We demonstrate that by using our algorithm a higher resolution recovery of the defect can be performed using partially coherent illumination without the need to increase the NA. Applying the algorithm to measurements of programmed defects of various sizes showed that defects appear to have both amplitude and phase.

## ACKNOWLEDGMENTS

This work performed in part at Lawrence Berkeley National Laboratory which is operated under the auspices of the Director, Office of Science, of the U.S. Department of Energy under Contract No. DE-AC02-05CH11231. This research was supported by collaboration with industry under the IMPACT+ program.

## **DISCLAIMER**

This document was prepared as an account of work sponsored by the United States Government. While this document is believed to contain correct information, neither the United States Government nor any agency thereof, nor The Regents of the University of California, nor any of their employees, makes any warranty, express or implied, or assumes any legal responsibility for the accuracy, completeness, or usefulness of any information, apparatus, product, or process disclosed, or represents that its use would not infringe privately owned rights. Reference herein to any specific commercial product, process, or service by its trade name, trademark, manufacturer, or otherwise, does not necessarily constitute or imply its endorsement, recommendation, or favoring by the United States Government or any agency thereof, or The Regents of the University of California. The views and opinions of authors expressed herein do not necessarily state or reflect those of the United States Government or any agency thereof or The Regents of the University of California.